Title

In-Situ/Operando X-ray Characterization of Metal Hydrides

Journal

ChemPhysChem, 20(10)

ISSN

1439-4235

Authors

Liu, Yi-Sheng
Jeong, Sohee
White, James L
et al.

Publication Date

2019-05-16

DOI

10.1002/cphc.201801185

Peer reviewed

In-Situ/Operando X-ray Characterization of Metal Hydrides

Yi-Sheng Liu[+],[a] Sohee Jeong[+],[b] James L. White,[c] Xuefei Feng,[a] Eun Seon Cho,[b, d] Vitalie Stavila,[c] Mark D. Allendorf,[c] Jeffrey J. Urban,*[b] and Jinghua Guo*[a, e]

In this article, the capabilities of soft and hard X-ray techniques, including X-ray absorption (XAS), soft X-ray emission spectroscopy (XES), resonant inelastic soft X-ray scattering (RIXS), X-ray photoelectron spectroscopy (XPS), and X-ray diffraction (XRD), and their application to solid-state hydrogen storage materials are presented. These characterization tools are indispensable for interrogating hydrogen storage materials at the relevant length scales of fundamental interest, which range from the micron scale to nanometer dimensions. Since nanostructuring is now well established as an avenue to improve the thermodynamics and kinetics of hydrogen release and uptake, due to properties such as reduced mean free paths of transport and increased surface-to-volume ratio, it becomes of critical importance to explicitly identify structure-property relationships on the nanometer scale. X-ray diffraction and spectroscopy are effective tools for probing size-, shape-, and structure-dependent material properties at the nanoscale. This article also discusses the recent development of in-situ soft X-ray spectroscopy cells, which enable investigation of critical solid/liquid or solid/gas interfaces under more practical conditions. These unique tools are providing a window into the thermodynamics and kinetics of hydrogenation and dehydrogenation reactions and informing a quantitative understanding of the fundamental energetics of hydrogen storage processes at the microscopic level. In particular, in-situ soft X-ray spectroscopies can be utilized to probe the formation of intermediate species, byproducts, as well as the changes in morphology and effect of additives, which all can greatly affect the hydrogen storage capacity, kinetics, thermodynamics, and reversibility. A few examples using soft X-ray spectroscopies to study these materials are discussed to demonstrate how these powerful characterization tools could be helpful to further understand the hydrogen storage systems.

1. Introduction

Consumption of fossil fuels has been a primary driver of global economic prosperity and industrialization; however, this has come at the cost of increased emissions of greenhouse gases, particularly carbon dioxide (CO_2), and other pollutants (SO_x, CO, NO_x, etc.).[1] The magnitude of these emissions' effects continues to increase as previously underdeveloped nations become industrialized and consumption intensifies in human activities such as commuting and travel, which heavily depend on hydrocarbon fuels.[2] Because of these issues, research and development activities focused on clean renewable energy sources have expanded substantially during the past two decades. The efforts include developing and utilizing efficient renewable energy sources that reduce undesired byproducts and simultaneously decrease the costs of production, transportation, and consumption of energy. Hydrogen is a promising clean energy carrier that can be readily converted to electricity by a fuel cell, with water as the only byproduct.[3] Hydrogen storage remains a particularly challenging task, particular for vehicular use.[4] Although hydrogen has the highest energy content of any common fuel by weight, the energy content by volume of both gaseous and liquid hydrogen is rather low. Higher energy densities could be attained if hydrogen could be reversibly stored in the solid-state, either in physisorbed form using nanoporous sorbents or in chemisorbed form in metal hydrides.[5]

Currently, there are three primary technologies under consideration for hydrogen storage: high-pressure compressed gas, cryogenically cooled gas, and solid-state materials (e.g., hydrides).[6] Although compressed gas storage is now used on some commercially available vehicles its volumetric capacity ($\approx 40\ g/L$) does not meet the long-term technical targets (50 g/L) identified by the U.S. Department of Energy (DOE). It also requires costly high-pressure compressors and carbon fiber-reinforced tanks, with the compression process itself consuming large amounts of energy.[7]

Alternatively, solid-state storage materials can potentially offer higher volumetric and gravimetric storage hydrogen capacities. Broadly speaking, there are two primary material classes of enduring interest that employ different hydrogen binding mechanisms: sorbents and metal hydrides. Among the

[a] *Dr. Y.-S. Liu,[+] Dr. X. Feng, Dr. J. Guo*
Advanced Light Source
Lawrence Berkeley National Laboratory
Berkeley, CA 94720, USA
E-mail: jguo@lbl.gov
[b] *Dr. S. Jeong,[+] Prof. E. Seon Cho, Dr. J. J. Urban*
Molecular Foundry
Lawrence Berkeley National Laboratory
Berkeley, CA 94720, USA
E-mail: jjurban@lbl.gov
[c] *Dr. J. L. White, V. Stavila, Dr. M. D. Allendorf*
Sandia National Laboratories
Livermore, CA 94551, USA
[d] *Prof. E. Seon Cho*
Department of Chemical and Biomolecular Engineering
Korea Advanced Institute of Science and Technology (KAIST)
[e] *Dr. J. Guo*
Department of Chemistry and Biochemistry
University of California, Santa Cruz, CA 95064, USA
[+] *Y.-S.L and S.J. contributed equally to this work*

most actively investigated materials are nanoporous metal organic framework (MOF)[8] sorbents and complex metal hydrides such as $Mg(BH_4)_2$.[9] These materials are attractive candidates for vehicular storage because of the lighter tank mass and lower storage pressures required compared with compressed gas. However, candidate materials still face challenges relating to their thermodynamics and kinetics of hydrogen uptake and release, as well as reversibility in the case of metal hydrides, which must be fundamentally understood and addressed to achieve widespread adoption in commercial onboard applications.

MOFs have open pores for H_2 physisorption with hydrogen capacities that correlate with their surface area and pore volume.[10] Unfortunately, cryogenic (77 K) temperatures are needed to achieve sufficient gravimetric and volumetric capacity due to the weak physisorption binding energies (typically < 10 kJ mol^{-1}).[8] Consequently, recent work on hydrogen storage in MOFs is aimed at increasing the working temperature by incorporating open metal sites, which have higher H_2 binding energies, and improving volumetric storage capacity by optimizing the surface area and pore volume.[11]

Metal hydrides absorb hydrogen through cleavage of the H–H bond and chemically binding the hydrogen atoms to form a new chemical compound. However, due to the relatively strong chemical bonds, high-capacity solid-state hydrides require substantially higher absorption/desorption temperatures than are practical for vehicular use (the DOE technical target for operating temperature range is 233 K–358 K). A number of strategies are under consideration to decrease the operating temperature, including nanostructuring and incorporation of dopants or additives.[12] However, it is becoming clear that a comprehensive understanding of phenomena at length scales beyond that of chemical bonds is needed before the problems associated with these materials can be solved. For example, although the initial formation of intermediate species and the effects of additives occur at sub-nm dimensions, the growth of product phases and mass transport occurs over tens of nm or more. Consequently, probing these systems, particularly under *in operando* conditions, is extremely challenging.

A variety of X-ray characterization techniques, using both soft and hard photons, can be employed to probe different properties and length scales in these systems. Soft X-rays, typically 100–5000 eV, have a short attenuation length (10 mm in air) and are often used to excite core electrons for chemical analysis spectroscopies of elements near the surface of a sample. Hard X-rays, those with energies above 5000 eV (5 keV), wavelengths on the scale of atomic spacings and radii and are typically used for structural studies using diffraction and scattering. Occasionally, an intermediate range called tender X-rays, often defined as 1000–5000 eV, has been designated as well.[13]

In this minireview, we orient the reader with background on solid-state metal hydrides, including their synthesis and the analysis of their hydrogen uptake capacity and dynamics. We then discuss the use of synchrotron-based X-ray spectroscopy capabilities to probe the fundamental mechanisms of hydrogen uptake and release in these materials. We then discuss the use of synchrotron-based X-ray spectroscopy capabilities to probe the fundamental mechanisms of hydrogen uptake and release in these materials. Importantly, these new in-situ cells can be operated under hydrogen uptake conditions and therefore enable the evolution of electronic structure to be probed in real time. As a characterization modality, X-ray based spectroscopic techniques provide an important complementary capability to traditional optical spectroscopy and NMR-based techniques due to the unique time- and energy scales they can probe.

2. Metal Hydride Synthesis, Hydrogen Uptake Capacity, and Dynamics

Metal hydrides are considered as potentially viable hydrogen storage materials because, in principle, they are able to provide much higher gravimetric capacities than sorbents or compressed gas at lower operating pressures.[9a,12b,14] For example, the gravimetric capacity of $Mg(BH_4)_2$ is 14.9 wt%, which cannot be matched by any known sorbent material, even at 77 K (although some organic frameworks now approach 10 wt% at cryogenic temperatures). However, the strong metal-hydrogen bonds often lead to unfavorable thermodynamics and slow reaction kinetics. This often necessitates the use of high desorption and regeneration temperatures and pressures. Moreover, long diffusion distances of hydrogen atoms through bulk materials further reduces performance.[9b,15] Experiments using thin films of metal hydride materials have shown that the kinetics of hydrogen storage can be enhanced by decreasing the diffusion path lengths for hydrogen,[16] motivating the reduction of the size of metal hydride materials to nanoscale dimensions as a promising approach to improve the performance in hydrogen storage.[17]

To obtain nanoscale metal hydride materials, there are two basic approaches: 1) top-down methods, such as a mechanical ball-milling, which start with bulk materials and subsequently produce smaller structures; and 2) bottom-up methods, which generate a larger and organized structure by self-assembly of atomic or molecular components. Ball-milling is an appealing top-down method because it allows scalable production at low cost. This method can produce nanomaterials of metal hydrides in 10–50 nm or larger crystalline size via mechanical fracture of their parent bulk crystals.[18] However, systematic control of the size distribution is difficult to achieve and aggregation of the resulting materials occurs, which makes achieving homogeneity a challenge. Consequently, bottom-up methods are preferable if uniform particles smaller than 10 nm are desired. Moreover, bottom-up approaches permit the use of additional supporting materials and functionality such as porous matrices, ligands, and wrapping functionalized carbon materials.[17a,b] Incorporation or encapsulation of supporting materials by melt infiltration, incipient wetness impregnation, and solution-based synthesis can prohibit aggregation and stabilize the particles, although there are fewer chemical degrees of freedom available.

The development of various nanostructuring synthetic methods for metal hydrides has lead to substantially improved hydrogen storage properties in terms of kinetics and thermodynamics.[19] Metal hydride nanomaterials have far larger surface areas (both solid-gas and solid-solid interfaces) and generate more energetically favorable phases than their bulk counterparts. This allows a greater portion of hydrogen atoms to have interfacial contact with the hydride-forming metal, leading to accelerated hydride formation within a reasonable range of operating temperatures. For example, Cho et al. recently reported exceptionally enhanced hydrogen storage properties by using a metal hydride nanocomposite composed of reduced graphene oxide and Mg nanoparticles (Mg/rGO).[15] The hydrogen absorption capacity of Mg/rGO nanoparticles with 3.25 nm ($\pm$0.87 nm) diameter was 7.56% H_2 in Mg nanoparticles, which is close to the theoretical value of 7.6 wt%. In addition, after several absorption/desorption cycles (250 °C/350 °C for 5 cycles and at 200 °C/300 °C for additional 20 cycles) the capacity and kinetics of Mg/rGO nanomaterials were well unchanged. This is attributed to the excellent stabilization of Mg nanomaterials without sintering or fracture, common phenomena known to reduce the hydrogen storage performance in bulk metal hydrides. Notably, rGO serves not only as a supporting material to stabilize nanomaterials, but also as an atomically thin protective layer for preventing serious oxidation of Mg nanomaterials. Thus, Mg nanomaterials encapsulated by rGO provide a new potential platform for the practical solid-state hydrogen storage.

3. Hard X-Ray Techniques

Hard X-ray techniques, such as powder X-ray diffraction (XRD), wide-angle X-ray scattering (WAXS), small angle X-ray scattering (SAXS), and pair distribution function (PDF) analysis, have been widely used for structural and morphological characterization of metal hydrides. Since metal hydrides are primarily comprised of low-Z elements, synchrotron radiation is often used as a high-intensity collimated light source to enhance sensitivity to these elements. Synchrotron radiation has certain advantages over lab-based sources, such as high flux and energy tunability, in both short-range and long-range structure analysis to understand the fundamental material properties and to guide new materials discovery efforts. In recent years, *in situ* and *in operando* techniques have been developed and offer high spatial and temporal resolution to enable real time dynamic investigation of structural changes in metal hydrides upon hydrogen cycling.[12b]

The term "powder" in "powder XRD" does not necessarily mean that the sample must be in powdered form, but rather that the crystalline domains are randomly oriented in the sample. When a 2-D diffraction pattern is collected, it shows concentric rings of scattering peaks corresponding to the various d-spacings in the crystal lattice, rather than the point spots observed for single crystals. The positions and the intensities of the peaks are used to identify the crystal structure and phase composition of the material. For example, bulk magnesium borohydride exhibits a rich structural chemistry and five different crystal structures (α-, β-, γ-, δ-, and ε-$Mg(BH_4)_2$) have been reported.[19] The phase identification of metal hydrides is important because their physical and chemical properties are highly dependent on the structure.[12b,21]

A variation of powder X-ray diffraction is grazing incidence XRD, typically used to characterize metal and metal hydride thin films.[16] The reflection geometry is used for these measurements, as the substrates are generally too thick for transmission. In this geometry, the incident angle to the sample is fixed at a small value exceeding the critical angle of total reflection; the angle between the incident beam and the diffracted beam (2θ) is varied by moving the detector. High angular resolution is required because the diffraction peaks from metal hydrides are often of low intensity. Consequently, multiple-bounce crystal monochromators are used to provide a highly collimated X-ray beam for these measurements.

WAXS is a diffraction experiment that consists of scanning large diffraction angles to cover a wide range of scattering variables down to small d-spacing, which corresponds roughly to the size of chemical bonds. In contrast, SAXS provides the ability to probe structural features over a much larger length scale corresponding to the size of crystalline ordering.[22] SAXS measurements are technically challenging because of the small angular separation of the direct beam and the scattered beam. Large specimen-to-detector distances (up to 10 meters) and high-quality collimating optics are used to achieve good signal-to-noise ratio. The SAXS technique is commonly used for probing larger length-scale structures such as nanoconfined metal hydrides[23] and metal hydride nanoparticles,[24] rather than the considerably smaller crystallographic planes typically examined with XRD.

Total scattering or pair distribution function (PDF) analysis is an analytical technique that can provide structural information from disordered materials by using the complete powder XRD pattern. Both the Bragg scattering and underlying diffuse scattering are employed. The X-ray pattern characterizes the long-range order of molecules and atoms in a material. Short-range order, such as the local interatomic structure, is present as less well-defined features. This local structure of metal hydrides (e.g., metal-metal distance) can be described quantitatively by the atomic PDF. Applications relevant to amorphous or nanoconfined metal hydrides have been recently discussed in a book chapter.[25] Many other examples of the applications of hard X-rays in structural determination of metal hydrides exist and we refer the reader to several excellent review articles on this topic.[26]

4. Soft X-Ray Spectroscopies

Soft X-ray spectroscopies are among the most powerful techniques available for probing the properties and mechanistic behavior of hydrogen storage materials, providing insights into their electronic structure and microstructure. Such techniques that have been employed for hydrogen storage research include X-ray absorption (XAS), X-ray emission (XES), and X-ray

photoelectron (XPS) spectroscopies, as well as resonant inelastic X-ray scattering (RIXS).[27] The bright and tunable X-ray beams available at third-generation synchrotron radiation facilities such as the Advanced Light Source (ALS) at Lawrence Berkeley National Laboratory enable material electronic structure to be characterized with both element-specific and chemical sensitivity (i.e., coordination environment, oxidation state). Moreover, soft X-ray spectroscopies are techniques that enable in-situ spectroscopic measurements under reaction conditions, such as hydrogenation and dehydrogenation processes in hydrogen storage materials.[28] In addition, among the synchrotron facilities worldwide such as BESSY II and SPRING-8, the ALS delivers the brightest soft X-rays and is developing in-situ soft X-ray spectroscopic capabilities optimized for energy science.[29]

The basic physics of XAS and XES are described in Figure 1. The core-electron X-ray absorption process is depicted in

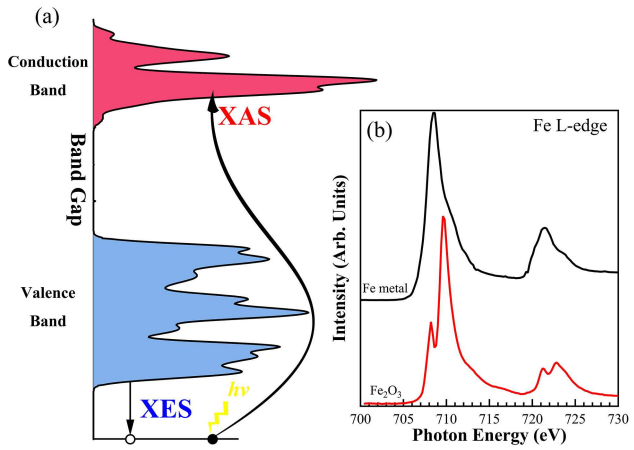

Figure 1. (a) Illustration of XAS and XES processes. (b) Fe L-edge XAS spectra of Fe metal (Fe^0) and Fe_2O_3 (Fe^{3+}).

Figure 1(a). Core electrons are excited by an incident X-ray photon to an unoccupied excited state in the conduction band, providing direct information about the electronic structure of this band. X-ray excitation transitions are no different than other electromagnetic excitations, being governed by the dipole selection rule requiring a change in angular momentum ($\Delta l = \pm 1$), which makes X-ray absorption a powerful tool for probing the electronic structure of specific core energy levels. For example, *3d* transition metal (TM) L-edges in XAS correspond to the excitation of a *2p* electron to a *3d* unoccupied orbital. TM *3d* orbitals are extremely sensitive to the oxidation state of the atom and the nature of the ligand-metal orbital hybridization near the Fermi level. Consequently, the XAS profile is strongly correlated with the physical and chemical properties of a material. This is illustrated in Figure 1(b), which shows the Fe L-edge XAS spectra of Fe metal and Fe_2O_3.[30] The lines shapes of the two are quite different, allowing one to distinguish Fe^0 from Fe^{3+}. These concepts can be extended to monitor the oxidation states of hydrogen storage materials during the uptake or release of hydrogen, which often involves a change in the redox state of the storage medium (e.g., in metal hydrides such as MgH_2, the Mg will go from a zero valence to a $+2$ charged state). In addition, XAS can be either surface-sensitive or bulk-sensitive by selecting the collection mode. Surface-sensitive total electron yield (TEY) measures the drain current to the sample surface, which has only a few nm probing depth. On the other hand, more bulk-sensitive total fluorescent yield (TFY) measures emitted photons from the sample and has a deeper probe depth of up to 100 nm. Hence, measuring the two yields simultaneously can be used to distinguish between surface and bulk properties within the system.[31] XPS is similar to XAS in that a core electron is excited; however, in XPS the electron is ejected from the material and its kinetic energy is measured to determine the binding energy of the orbital from which it originated. Because XPS, like the TEY mode of XAS, involves electrons rather than photons, it is very surface-sensitive.[32]

It should be mentioned that, since XAS is very sensitive to materials' chemical environment (particularly in TEY mode), proper sample preparation and handling are critical to ensure that the samples are studied as intended rather than in a degraded form. The typical highly unstable materials, e.g., battery materials or metal hydrides, tend to react with water vapor and other gases if exposed to air during the sample preparation. Improper sample handling for those air-sensitive samples can easily result in contaminated XAS spectra and lead to incorrect conclusions. One of the examples is the study of solid electrolyte LLZO which has been examined by exposing the sample to air intentionally. The XAS spectra show significant differences depending on what gas has been exposed to the sample.[33]

In addition, the self-absorption or saturation effect can be problematic for quantitative data analysis in XAS, as these phenomena can result in quenching of XAS spectral features especially for XAS data recorded in TFY detection mode (in contrast to that from TEY detection mode). The self-absorption effect is due to the re-absorption of the emitted photons by adjacent atoms in bulk from the initially measured atom. As a consequence, the TFY photon detector artificially detects much lower counts at the absorption maximum than occurs in reality. In general, TFY XAS spectra can be used for diluted samples without much concern of self-absorption effect as self-absorption scales with path length. Also, in many cases the self-absorption effect can be either corrected by a mathematical process with the known physical properties of the materials.[34] Technically, the self-absorption effect can also be eliminated experimentally by measuring IPFY (inverse partial fluorescence yield) detection mode. Detailed information regarding self-absorption-free XAS spectra utilizing a solid-state dispersive detector[5] or RIXS spectrometer can be found in other literature.[36]

Conversely, XES is a de-excitation process of core-hole excited states.[37] The core-excited-hole state created following the X-ray absorption process will be refilled by a valence electron and emit an X-ray photon. Hence, XES probes the occupied electronic states in the valence band and provides electronic structure information such as the partial density of

states (pDOS).[38] Monitoring the pDOS provides tremendous insight into the evolution of local electronic structure during the hydrogen storage process. For example, many hydride materials transform from a metal (e.g., Li, Mg) into a semiconductor (e.g., LiH, MgH_2).

RIXS (Resonant Inelastic X-ray Scattering) is a series of processes that involve core-electron excitations in the materials and detects the inter/intra-atomic excitations related to chemical processes. A feature of RIXS is that the de-excitation channels can be open to various collective excitations. Many of the excitation/de-excitation processes associated with RIXS can provide valuable insight into the chemistry of complex hydrides. For example, information concerning charge transfer (CT), *d-d* excitations,[39] and electron-phonon coupling[40] that occur in response to sorption or desorption can be obtained. A downside of RIXS is that it is a photon-hungry process due to its low yield of inelastic scattering. Therefore, it requires high incident X-ray fluence, which can potentially damage sensitive materials with bright X-rays illumination. It also relies on advanced detectors to increase data acquisition speed and quality. Reducing data collection time under in-situ/operando conditions is crucial to observe the transient, time-dependent intermediate states that emerge during the hydrogenation process. One significant advance in this area is the development of high-resolution, high-throughput RIXS spectrometers and new variable line-spacing (VLS) X-ray emission spectrometers. These have recently been employed on beamline 8.0.1 at the ALS.[41] Generally speaking, the RIXS data acquisition time with the VLS spectrometer is hundreds of times faster than measurements using older grazing-angle Roland-type spectrometers. Also, with improved spectrometer efficiency and much higher energy resolution, RIXS mapping, partial fluorescence yield, and inverse partial fluorescence yield XAS can be achieved.[36]

5. In Situ Measurements

In the following section, the terms "in situ" and "in operando" are used to refer to measurements taken under conditions, particularly temperature and pressure, similar to, if not duplicating, those that would be present in actual operation. In-situ X-ray spectroscopies are very useful in probing energy and catalysis materials whose activity involves the behavior of solids with either gases or liquids..

Due to the short penetration length of soft X-rays in ambient atmosphere (~10 mm), spectroscopic experiments are typically performed in an ultrahigh vacuum (UHV) chamber. This requirement becomes a challenge for conducting in-situ soft X-ray spectroscopy in involving solid/liquid or solid/gas interactions and interfaces-precisely the sorts of environments where historically challenging questions regarding the chemistry of hydrogen storage materials arise. In principle, *in operando* soft X-ray spectroscopy could elucidate currently unknown details of bonding and electronic structure perturbations that occur during hydrogenation or dehydrogenation. Tremendous effort has been invested at many synchrotron facilities worldwide over the past few decades to develop in-situ soft X-ray capabilities that allow dynamic processes to be observed.[42]

One key-enabling component of in-situ X-ray studies is the membrane window that encloses the in-situ cell. In contrast to optical in-situ studies, which often use quartz or sapphire, the criteria for an X-ray transmissive membrane are multifaceted. Of course, the membrane window must be transparent to the beam to allow X-rays to interact with samples and emitted photons to be detected; thus, a large energy window of transparency is required (Figure 2). However, the transmission

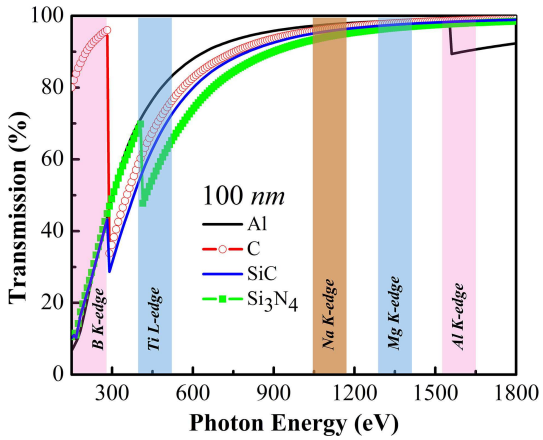

Figure 2. X-ray transmission of 100 nm thick X-ray membrane with various materials at incident photon energy. Data obtained from the Center for X-Ray Optics (CXRO). Reproduced with permission from Ref. [44]

rate of X-rays through materials is strongly dependent on the energy of the X-ray photons and the chemical composition and thickness of the membrane material. Typical thicknesses of the soft X-ray membranes used in most of the experiments is about 100 nm, and the majority of membrane materials are composed of Al, C, SiC, or Si_3N_4. The soft X-ray transmission rate vs. photon energy profiles for these materials are shown in Figure 2. In this figure, the colored areas indicate the corresponding elemental absorption edges relevant to hydrogen storage materials e.g., B, O, and Mg K-edges have ~30%, 60%, and 95% transmission with a 100 nm thick Si_3N_4 membrane, respectively. Therefore, the membrane material must be carefully chosen depending on the element of interest in the specific hydrogen storage system.

Soft X-ray membrane windows also separate the sample in an environment of gas or liquid from the UHV experimental chamber and must therefore withstand the pressure differential between vacuum and the ambient pressure of the in-situ cell. Historically, the thin (~100 nm) membranes limited the possible pressures used for in-situ studies. Recently, however, a 100 nm thick, 5×5 μm Si_3N_4 X-ray membrane with sufficient mechanical strength to withstand the pressure differential was developed that allows liquid pressures up to 100 bar.[43] It is also suitable to sustain a high-pressure gas environment with appropriate safety protections. This breakthrough could make in-situ soft X-ray spectroscopy experiments possible for the first time with

hydrogen storage materials that operate under high hydrogen gas pressure conditions, such as $Mg(BH_4)_2$.

In-situ XPS experiments have also been conducted on a variety of storage materials, including both electrochemical[45] and hydride[47] energy materials. Two different approaches are employed to probe systems with gas or liquid present at the solid interface. In ambient-pressure XPS (AP-XPS), the sample is placed in a chamber at gas pressures up to about 20 Torr. A narrow aperture leading through a set of differentially pumped chambers to the analyzer, which is kept at UHV conditions, is situated very close to the surface of the sample to collect photoelectrons before they are scattered by the gas molecules. The high intensity of synchrotron radiation is particularly useful for AP-XPS in overcoming decreased signal due to scattering at elevated pressures. Additionally, thermal or electrochemical control can be applied to drive a particular reaction *in operando*. AP-XPS enables the sampling of the solid, gas, and liquid (if present) simultaneously, though the different signals have to be deconvoluted accurately for proper analysis. Another recently developed approach is the use of a thin membrane, as in *in situ* XAS, which separates the UHV chamber with the X-ray source from another kept at pressures up to 1 bar.[27b] However, due to the surface sensitivity of XPS, the membrane itself must be the material analyzed, and often it is semi-permeable or even partially reactive to the gas applied to the pressurized side so that changes can be detected on the UHV side without rupturing the membrane. A common example of this is palladium in a hydrogen environment, since Pd readily forms a hydride with tunable stoichiometry based on the applied pressure.[46] This membrane-based approach is useful for lab-based systems without the high flux of a synchrotron and the specialized differential pumping setup required for AP-XPS, since the incident X-rays and the photoelectrons are maintained in a UHV environment.

5.1. In Situ Gas Flow Cells

An XAS gas flow cell is designed for soft X-ray spectroscopy studies of solid/gas interfaces in reactions such as the Fischer-Tropsch process,[47] the direct catalytic reduction of NO[48] and other harmful gases,[49] and hydrogen storage applications. The current gas flow cell employed at the ALS operates at a gas pressure of 1 bar with a temperature range from 25 °C up to 300 °C. However, since many solid-state hydrogen storage materials can only be hydrogenated at high pressures (up to hundreds of bar), which are much greater than the maximum working pressure of the current gas cell, typically only hydrogenation events that occur on the surface are investigated since there is insufficient gas pressure to drive H completely into the bulk. Therefore, intriguing comparisons can be made between XAS operating in the more surface-sensitive total electron yield (TEY) mode and the more bulk-sensitive total fluorescence yield (TFY).

To study the H_2 adsorption and desorption processes at the surface/interface, we constructed in-situ cells for soft X-ray characterization of solid-state hydrides. A detailed schematic drawing of an in-situ gas flow cell is shown in Figure 3a. The membrane window is mounted and sealed using O-rings in the front of the cell. A grooved Au-coated sample stage is located behind the membrane window with a gap of approximately 200 μm between the two, and this gap allows gas flow through the sample surface. A cartridge heater in contact with the sample stage allows for heating of the sample up to 300 °C. An improved version of the in-situ gas flow cell is under development in order to meet the needs of studying solid-state hydrogen storage and catalysis materials at higher temperatures (up to 500°C) and higher gas pressure (tens to hundreds of bar). In addition, the development of in-situ soft X-ray spectroscopy cells for solid-gas reactions can be found in some other synchrotron facilities worldwide. For example, an in-situ gas flow cell for scanning transmission X-ray microscopy (STXM) was developed by de Smit et al. They utilize this transmission gas flow cell to study Fischer–Tropsch synthesis on supported iron oxide under a mixture of CO and H_2 (1 bar) at 350°C by scanning a region of the material and probing the X-ray absorption at the O K-edge and the Fe L-edge.[50] A few more different studies regarding to the use and developments of in-situ soft x-ray gas flow cell can be found in the literature.[51] In contrast, hard X-rays, which are much more penetrating, can be utilized in the presence of an atmosphere which makes the in-situ setup much simpler than in soft X-ray techniques. For example, Zhang et al. have developed an in-situ gas flow cell for use in hard X-ray absorption spectroscopy to study oxidation of carbon monoxide on Pt/Al_2O_3 catalysts.[51c]

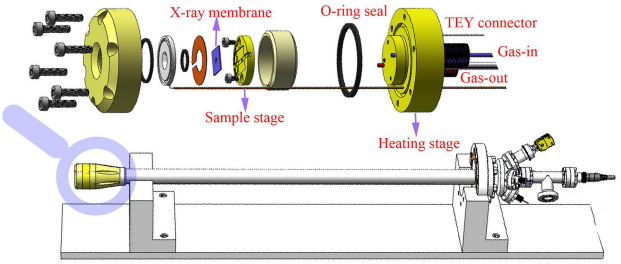

Figure 3. Soft X-ray high-temperature in-situ gas flow cell.

6. Examples

6.1. Ti-Catalyzed Sodium Alanate ($NaAlH_4$)

Complex metal hydrides represent one of the most attractive classes of hydrogen storage materials. Since most of binary metal hydrides form metal-hydrogen covalent bonds that have large enthalpies, relatively high temperature are required to transform to the dehydrogenated state.[52] The complex metal hydrides that have been considered as potential candidates for hydrogen storage application include $NaAlH_4$, owing to its light weight and potential for reversibility.[5a] Within the AlH_4^- anion, the Al atom covalently bonds to four hydrogen atoms, and the anion ionically bonds to the Na^+ cation, yielding a fairly stable

compound. Small quantities of transition metal additives can greatly improve the kinetics and thermodynamics of complex metal hydrides. For example, Ti-catalyzed $NaAlH_4$ shows different equilibrium points with different Ti contents and exhibits good reversibility in cyclic hydrogenation/dehydrogenation, whereas the undoped material cannot readily be rehydrogenated.[53]

The Al K-edge XAS spectra of 2 mol% $TiCl_3$-catalyzed $NaAlH_4$ was measured in TEY mode at various hydrogenation levels (as-mixed, as-synthesized by ball-milling for two hours, dehydrogenated, and re-hydrogenated samples) along with Al metal and Al_2O_3 as reference for comparison (Figure 4a). The as-mixed

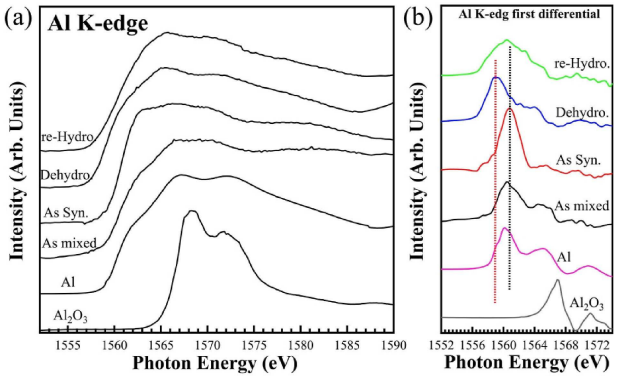

Figure 4. Al K-edge TEY XAS spectra of Ti-$NaAlH_4$ at different conditions. (b) First differentials of the spectra in (a).

sample consists of physically mixed 2 mol% $TiCl_3$ and $NaAlH_4$, compared to the reactive high-energy ball-milling in the as-synthesized sample. The Al K-edge spectra of the as-mixed and as-synthesized samples indicate a change in the Al chemical environment at the surface after ball milling. The TEY XAS spectrum of the as-synthesized sample exhibits a strong shoulder feature at 1562 eV, which resembles the Al metallic-like structure. Thus, it is evident that the high-energy ball milling induces the reaction of $TiCl_3$ with $NaAlH_4$ to form metallic-like Al species on the surface.

Upon dehydrogenation, the AlH_4^- symmetry breaks down from the release of chemically bonded H, causing the Al XAS spectral edge to be shifted toward lower energy than even the metallic phase on the surface. Figure 4b shows the first differential curves of the Al K-edge spectra, which can easily distinguish the spectral shift for all the samples. The results indicate that the dehydrogenated sample shifts toward lower photon energy than even pure Al metal. This implies that the system tends to formation of ionic species, such as Na_3AlH_6, upon hydrogen release, since the shifting of XAS spectra to lower-energies are often observed with the change to lower oxidation states. Once the sample is re-hydrogenated, the dehydrogenated and hydrogenated species co-exist according to the broad green curve in Figure 4b. The XAS spectrum of the re-hydrogenated sample does not match that of the as-synthesized sample, which suggests that significant changes occur in the material after a full cycle of hydrogen release and absorption. Possible re-hydrogenation pathways could lead to the formation of pure Al, $NaAlH_4$, Na_3AlH_6 and NaH. Figure 5a shows the Na K-edge XAS spectra of the $NaAlH_4$ samples, as well as metallic Na for comparison. The Na spectrum shifts slightly to higher energy upon dehydrogenation, which indicates changes in the chemical environment around Na at various stages of the reaction, with the strongly ionic bonding character characteristic for NaH and Na_3AlH_6. It is consistent with the behavior of Al K-edge XAS spectra that the Al has a strong ionic bonding upon dehydrogenation. Furthermore, Ti L-edge XAS spectra in Figure 5b show that Ti is most similar after ball milling to Ti metal and retains the same state throughout the hydrogenation and dehydrogenation processes.

6.2. Mg Hydrides

Magnesium-based hydrides are considered promising candidates for solid-state hydrogen storage due to high gravimetric storage density (7.6 wt% for MgH_2, 14.9 wt% for $Mg(BH_4)_2$). However, their utilization is hampered by the high operating temperatures required, slow reaction kinetics, and poor air-stabilities. Several review articles have been published in recent years on hydrogen storage properties of both binary and

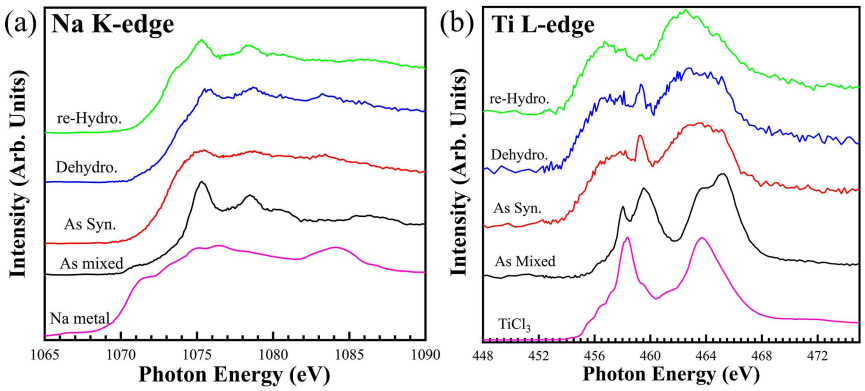

Figure 5. (a) Na K-edge and (b) Ti L-edge XAS spectra of Ti-$NaAlH_4$ at different conditions of hydrogenation.

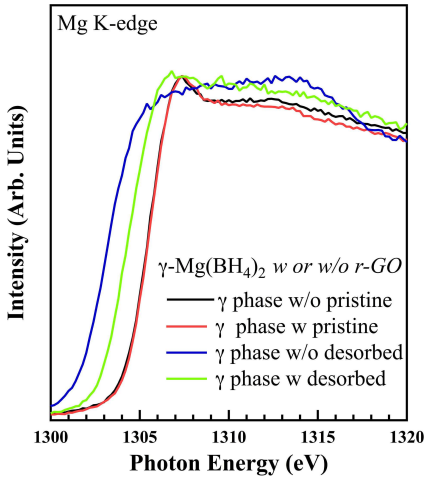

Figure 6. Mg K-edge XAS spectra of $Mg(BH_4)_2$ with or without rGO encapsulation.

complex Mg-based metal hydrides.[21,54] One of the most promising strategies to improve the properties of these hydrides is to reduce their critical dimensions to the nanoscale, for example by incorporating hydride nanoparticles with graphene, reduced graphene oxide (rGO), and graphene nano ribbon (GNR), which improve the kinetics and protect against oxidation by O_2 or H_2O.[55]

6.2.1. $Mg(BH_4)_2$

The experimental Mg K-edge XAS spectra of pristine and dehydrogenated gamma-phase $Mg(BH_4)_2$ samples with and without rGO encapsulation are shown in Figure 6 The Mg K-edge XAS spectral shape of these samples is nearly identical (black and red curves). Therefore, the encapsulation does not significantly affect the chemical environment of the Mg. However, the XAS spectra of hydrogen-desorbed samples with and without rGO are clearly different; the spectral edge shows an energy-shift towards lower photon energy side for the sample without rGO coverage. This shift is attributed to the existence of MgB_2 (not shown here but can be found in ref. 18) and is expected to be absent in kinetic byproducts such as $MgB_{12}H_{12}$ spectrum.[56] Hence, these results imply that the sample without rGO dehydrogenates to MgB_2 without forming significant amount of byproducts such as $MgB_{12}H_{12}$. The less-shifted spectrum of the desorbed sample with rGO indicates a possible formation of MgH_2, which indicates that the dehydrogenation pathway could be different for the samples with and without rGO.

6.2.2. rGO Encapsulated Mg Nanocomposites

Magnesium nanoparticles possess high hydrogen adsorption capacity and reversibility, especially at the nanoscale due to the increase of surface area. However, they are very chemically active to the environment, which makes them unrealistic for hydrogen-storage applications. With state-of-art material engineering, Mg nanoparticles covered with highly porous rGO has been synthesized.[15] The rGO layers act as protection to prevent O_2 and H_2O from reacting with the contained Mg nanoparticles while allowing hydrogen to penetrate through and transforming them to magnesium hydride. Mg@rGO has shown extraordinary hydrogen storage capacity of ~7 wt% at 15 bar of hydrogen and 250°C with excellent reversibility. The ex-situ Mg K-edge XAS has been applied to characterize the electronic structure at the hydrogenation condition and shown in Figure 7a. The Mg K-edge XAS spectra exhibit a spectral shift to

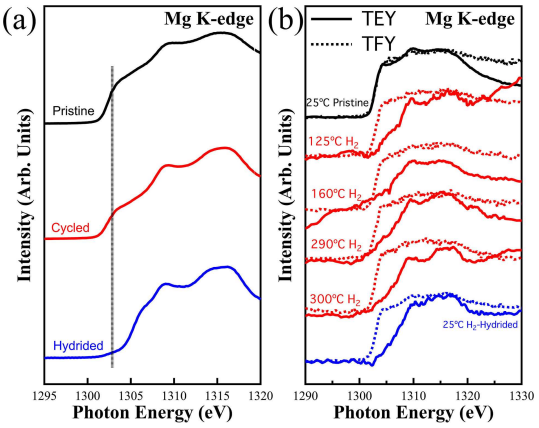

Figure 7. (a) Ex-situ Mg K-edge XAS and (b) temperature dependent in-situ Mg K-edge XAS spectra of Mg nanocomposites encapsulated by rGO.

higher energy, which is attributed to the formation of higher valence MgH_2. Previously published XRD results show that the rGO layers readily prevent further oxidation under the ambient condition for a period of time up to a few months. However, recent theoretical calculation reveals that an ultra-thin oxide layer of MgO in a honeycomb-like structure might be formed even with rGO encapsulation, and, surprisingly, this thin oxide layer facilitates hydrogen storage and reversibility.[57]

The ex situ Mg K-edge XAS characterizations in UHV reveal spectral differences between hydrogenated and dehydrogenated species, which motivate the probing of the evolution of electronic structure in-situ during the hydrogenation process. In this case, the Mg@rGO nanoparticles were pressed and loaded in the previously discussed gas flow cell. The gas flow cell was purged with N_2 for 12 hours prior to the measurements to remove possible gas residues in the cell. The Mg K-edge XAS spectra were measured in both TEY and TFY mode simultaneously. The first Mg K-edge XAS spectrum was recorded at room temperature with a continuous flow of H_2 in the cell. Thereafter, the samples were heated up to 300 °C while flowing H_2 at pressure of 1 bar, and XAS spectra were recorded at various temperatures,[12a] as shown in Figure 7b. The intensity of the significant shoulder at ~1303 eV in the TEY-recorded XAS spectrum begins to decrease when the temperature reaches 150°C in comparison with the ex-situ measurement shown in Figure 7a. This shows that the formation of MgH_2 starts at

relatively low temperature in H_2 environment at pressure of 1 bar. Surface-sensitive TEY detection provides additional useful insight since under the low pressure used in this experiment bulk MgH_2 is unlikely to form. On the contrary, the TFY XAS spectra are similar at all temperatures. It is thus evident that the hydrogenation process only occurs on the surface because TFY showed only the spectrum corresponding to bulk Mg because its probing depth exceeds 100 nm.

At a temperature of 300 °C, the shoulder feature disappears completely in the TEY spectrum, indicating that the Mg nanoparticles are fully hydrogenated to MgH_2 on the surface. Based on the previous study of H_2 uptake at 15 bar H_2 and 250 °C,[15] only ~1 wt% of H_2 is stored in the Mg nanoparticles under H_2 pressure of 1 bar. This example (Figure 7b) powerfully demonstrates the sensitivity of in-situ soft X-ray spectroscopy to the hydrogenation state of Mg-containing hydrides.

7. Summary

The application of in-situ X-ray methodologies can provide valuable insight into the evolution of chemical bonding and electronic structure in storage materials as they absorb and release hydrogen. In-situ gas flow cells, such as the one described above, are powerful tools for extending soft X-ray spectroscopies to probe the electronic structure of solid/gas interfaces under hydrogenation and dehydrogenation conditions. Insights derived from these cutting-edge approaches are needed to develop new solid-state hydrogen storage materials that are practical alternatives to high-pressure gas. In particular, they can assist in filling the gap in understanding of the hydrogenation and dehydrogenation mechanisms at the conditions approaching operating pressures of hydrogen refueling stations. One important scientific hurdle – understanding the intermediate states that occur during hydrogenation processes – can be addressed with in-situ synchrotron techniques. This is essential for developing synthetic approaches to mitigate thermodynamic and kinetic traps that prevent promising materials from meeting DOE technical targets.

Acknowledgements

The authors gratefully acknowledge research support from the Hydrogen Materials Advanced Research Consortium (HyMARC), established as part of the Energy Materials Network by the U.S. Department of Energy, Office of Energy Efficiency and Renewable Energy, Fuel Cell Technologies Office. Work at the Molecular Foundry, Lawrence Berkeley National Laboratory, was supported by the Department of Energy, Office of Science, Office of Basic Energy Sciences, Scientific User Facilities Division of the U.S. Department of Energy under Contract No. DE-AC02-05CH11231. The X-ray spectroscopy experiments discussed were performed on BL7.3.1 (XAS endstation) and BL8.0.1.4 (wetRIXS endstation) at the Advanced Light Source, which is supported by the Office of Science of the U.S. Department of Energy under Contract No. DE-AC02-05CH11231. Part of the work was supported by International Energy Joint R&D Program of the Korea Institute of Energy Technology Evaluation and Planning (KETEP), granted financial resource from the Ministry of Trade, Industry & Energy, Republic of Korea (No. 20188520000570). Sandia National Laboratories is a multimission laboratory managed and operated by National Technology and Engineering Solutions of Sandia, LLC., a wholly owned subsidiary of Honeywell International, Inc., for the U.S. Department of Energy's National Nuclear Security Administration under contract DE-NA-0003525. This paper describes objective technical results and analysis. Any subjective views or opinions that might be expressed in the paper do not necessarily represent the views of the U.S. Department of Energy or the United States Government.

Conflict of Interest

The authors declare no conflict of interest.

[1] L. Chapman, *Journal of Transport Geography* **2007**, *15*, 354–367.
[2] a) C. McGlade, P. Ekins, *Nature* **2015**, *517*, 187–190; b) K. Anderson, *Nature Geoscience* **2015**, *8*, 898.
[3] a) D. Ipsakis, S. Voutetakis, P. Seferlis, F. Stergiopoulos, C. Elmasides, *Int. J. Hydrogen Energy* **2009**, *34*, 7081–7095; b) E. L. V. Eriksson, E. M. Gray, *Appl. Energy* **2017**, *202*, 348–364.
[4] a) D. K. Ross, *Vacuum* **2006**, *80*, 1084–1089; b) M. Felderhoff, C. Weidenthaler, R. von Helmolt, U. Eberle, *Phys. Chem. Chem. Phys.* **2007**, *9*, 2643–2653.
[5] a) B. Sakintuna, F. Lamari-Darkrim, M. Hirscher, *Int. J. Hydrogen Energy* **2007**, *32*, 1121–1140; b) M. Sevilla, R. Mokaya, *Energy Environ. Sci.* **2014**, *7*, 1250–1280.
[6] a) H. M. Y. Kojima, T. Ichikawa L. S. Steven, in *New and future developments in catalysis*, **2013**, p. 99; b) A. Züttel, *Mater. Today* **2003**, *6*, 24–33.
[7] L. Schlapbach, A. Zuttel, *Nature* **2001**, *414*, 353–358.
[8] M. P. Suh, H. J. Park, T. K. Prasad, D.-W. Lim, *Chem. Rev.* **2012**, *112*, 782–835.
[9] a) V. Stavila, L. Klebanoff, J. Vajo, P. Chen, in *Hydrogen Storage Technology*, CRC Press, **2012**, pp. 133–212; b) S.-i. Orimo, Y. Nakamori, J. R. Eliseo, A. Züttel, C. M. Jensen, *Chem. Rev.* **2007**, *107*, 4111–4132.
[10] a) B. Panella, M. Hirscher, S. Roth, *Carbon* **2005**, *43*, 2209–2214; b) J. Goldsmith, A. G. Wong-Foy, M. J. Cafarella, D. J. Siegel, *Chem. Mater.* **2013**, *25*, 3373–3382; c) M. D. Allendorf, Z. Hulvey, T. Gennett, A. Ahmed, T. Autrey, J. Camp, E. Seon Cho, H. Furukawa, M. Haranczyk, M. Head-Gordon, S. Jeong, A. Karkamkar, D.-J. Liu, J. R. Long, K. R. Meihaus, I. H. Nayyar, R. Nazarov, D. J. Siegel, V. Stavila, J. J. Urban, S. P. Veccham, B. C. Wood, *Energy Environ. Sci.* **2018**, *11*, 2784–2812.
[11] J. Ren, N. M. Musyoka, H. W. Langmi, M. Mathe, S. Liao, *Int. J. Hydrogen Energy* **2017**, *42*, 289–311.
[12] a) E. S. Cho, A. M. Ruminski, Y.-S. Liu, P. T. Shea, S. Kang, E. W. Zaia, J. Y. Park, Y.-D. Chuang, J. M. Yuk, X. Zhou, T. W. Heo, J. Guo, B. C. Wood, J. J. Urban, *Adv. Funct. Mater.* **2017**, 1704316; b) A. Schneemann, J. L. White, S. Kang, S. Jeong, L. F. Wan, E. S. Cho, T. W. Heo, D. Prendergast, J. J. Urban, B. C. Wood, M. D. Allendorf, V. Stavila, *Chem. Rev.* **2018**, *118*, 10775–10839.
[13] D. Attwood, *Soft X-Rays and Extreme Ultraviolet Radiation*, Cambridge University Press, **1999**.
[14] U. Eberle, G. Arnold, R. von Helmolt, *J. Power Sources* **2006**, *154*, 456–460.
[15] E. S. Cho, A. M. Ruminski, S. Aloni, Y.-S. Liu, J. Guo, J. J. Urban, *Nat. Commun.* **2016**, *7*, 10804.

[16] a) K. Suzuki, *Journal of the Less Common Metals* **1983**, *89*, 183–195; b) A. Baldi, B. Dam, *J. Mater. Chem.* **2011**, *21*, 4021–4026.

[17] a) P. E. de Jongh, P. Adelhelm, *ChemSusChem* **2010**, *3*, 1332–1348; b) R. Mohtadi, S.-i. Orimo, *Nat. Rev. Mater.* **2016**, *2*, 16091; c) J. J. Vajo, *Curr. Opin. Solid State Mater. Sci.* **2011**, *15*, 52–61; d) T. K. Nielsen, F. Besenbacher, T. R. Jensen, *Nanoscale* **2011**, *3*, 2086–2098; e) M. U. Niemann, S. S. Srinivasan, A. R. Phani, A. Kumar, D. Y. Goswami, E. K. Stefanakos, *Journal of Nanomaterials* **2008**, *2008*, 9.

[18] V. Bérubé, G. Radtke, M. Dresselhaus, G. Chen, *Int. J. Energy Res.* **2007**, *31*, 637–663.

[19] H. Reardon, J. M. Hanlon, R. W. Hughes, A. Godula-Jopek, T. K. Mandal, D. H. Gregory, *Energy Environ. Sci.* **2012**, *5*, 5951–5979.

[20] a) Y. Filinchuk, R. Černý, H. Hagemann, *Chem. Mater.* **2009**, *21*, 925–933; b) J.-H. Her, P. W. Stephens, Y. Gao, G. L. Soloveichik, J. Rijssenbeek, M. Andrus, J.-C. Zhao, *Acta Crystallogr. Sect. B* **2007**, *63*, 561–568; c) W. I. F. David, S. K. Callear, M. O. Jones, P. C. Aeberhard, S. D. Culligan, A. H. Pohl, S. R. Johnson, K. R. Ryan, J. E. Parker, P. P. Edwards, C. J. Nuttall, A. Amieiro-Fonseca, *Phys. Chem. Chem. Phys.* **2012**, *14*, 11800–11807; d) L. George, V. Drozd, S. K. Saxena, E. G. Bardaji, M. Fichtner, *J. Phys. Chem. C* **2009**, *113*, 486–492; e) Y. Filinchuk, B. Richter, T. R. Jensen, V. Dmitriev, D. Chernyshov, H. Hagemann, *Angew. Chem. Int. Ed.* **2011**, *50*, 11162–11166; *Angew. Chem.* **2011**, *123*, 11358–11362; f) B. Richter, D. B. Ravnsbæk, N. Tumanov, Y. Filinchuk, T. R. Jensen, *Dalton Transactions* **2015**, *44*, 3988–3996; g) M. Dimitrievska, J. L. White, W. Zhou, V. Stavila, L. E. Klebanoff, T. J. Udovic, *Phys. Chem. Chem. Phys.* **2016**, *18*, 25546–25552.

[21] O. Zavorotynska, A. El-Kharbachi, S. Deledda, B. C. Hauback, *Int. J. Hydrogen Energy* **2016**, *41*, 14387–14403.

[22] T. Li, A. J. Senesi, B. Lee , *Chem. Rev.* **2016**, *116*, 11128–11180.

[23] S. Sartori, K. D. Knudsen, A. Roth, M. Fichtner, B. C. Hauback, *Nanoscience and Nanotechnology Letters* **2012**, *4*, 173–177.

[24] P. K. Pranzas, M. Dornheim, U. Bosenberg, J. R. Ares Fernandez, G. Goerigk, S. V. Roth, R. Gehrke, A. Schreyer, *J. Appl. Crystallogr.* **2007**, *40*, s383-s387.

[25] L. Malavasi, *Chapter 7: Structure of Crystallographically Challenged Hydrogen Storage Materials from Total Scattering*, CRC Press, **2016**.

[26] a) R. Cerný, *Mater. Sci. Forum* **1996**, *228–231*, 677–682; b) W. Kaysser, J. Esslinger, V. Abetz, N. Huber, K. U. Kainer, T. Klassen, F. Pyczak, A. Schreyer, P. Staron, *Adv. Eng. Mater.* **2011**, *13*, 637–657; c) V. Yartys, R. Denys, J. P. Maehlen, C. J. Webb, E. M. Gray, T. Blach, A. A. Poletaev, J. K. Solberg, O. Isnard, *MRS Proceedings* **2011**, *1262*, 1262-W1204-1201; dJ. Huot, D. B. Ravnsbæk, J. Zhang, F. Cuevas, M. Latroche, T. R. Jensen, *Prog. Mater. Sci.* **2013**, *58*, 30–75.

[27] a) R. Delmelle, J. C. Gehrig, A. Borgschulte, A. Züttel, *AIP Adv.* **2014**, *4*, 127130; b) O. Sambalova, A. Borgschulte, *J. Alloys Compd.* **2018**, *742*, 518–523.

[28] a) J. Guo, P.-a. Glans, Y.-s. Liu, C. Chang, in *On Solar Hydrogen & Nanotechnology*, John Wiley & Sons, Ltd, **2010**, pp. 123–142; b) H. Liu, Guo, Y. Yin, A. Augustsson, C. Dong, J. Nordgren, C. Chang, P. Alivisatos, G. Thornton, D. F. Ogletree, F. G. Requejo, F. de Groot, M. Salmeron, *Nano Lett.* **2007**, *7*, 1919–1922.

[29] J. Guo, *J. Electron Spectrosc. Relat. Phenom.* **2013**, *188*, 71–78.

[30] a) F. M. F. de Groot, J. C. Fuggle, B. T. Thole, G. A. Sawatzky, *Phys. Rev. B* **1990**, *42*, 5459–5468; b) X. Liu, J. Liu, R. Qiao, Y. Yu, H. Li, L. Suo, Y. S. Hu, Y. D. Chuang, G. Shu, F. Chou, T. C. Weng, D. Nordlund, D. Sokaras, Y. J. Wang, H. Lin, B. Barbiellini, A. Bansil, X. Song, Z. Liu, S. Yan, G. Liu, S. Qiao, T. J. Richardson, D. Prendergast, Z. Hussain, F. M. de Groot, W. Yang, *J. Am. Chem. Soc.* **2012**, *134*, 13708–13715.

[31] A. J. Achkar, T. Z. Regier, H. Wadati, Y. J. Kim, H. Zhang, D. G. Hawthorn, *Phys. Rev. B* **2011**, *83*, 081106.

[32] W. F. S. J. F. Moulder, P. E. Sobol, K. D. Bomben, *Handbook of X-ray Photoelectron Spectroscopy*, **1992**.

[33] L. Cheng, E. J. Crumlin, W. Chen, R. Qiao, H. Hou, S. Franz Lux, V. Zorba, R. Russo, R. Kostecki, Z. Liu, K. Persson, W. Yang, J. Cabana, T. Richardson, G. Chen, M. Doeff, *Phys. Chem. Chem. Phys.* **2014**, *16*, 18294–18300.

[34] B. Ravel, M. Newville, *J. Synchrotron Radiat.* **2005**, *12*, 537–541.

[35] A. J. Achkar, T. Z. Regier, E. J. Monkman, K. M. Shen, D. G. Hawthorn, *Sci. Rep.* **2011**, *1*, 182.

[36] R. Qiao, Q. Li, Z. Zhuo, S. Sallis, O. Fuchs, M. Blum, L. Weinhardt, C. Heske, J. Pepper, M. Jones, A. Brown, A. Spucces, K. Chow, B. Smith, P. A. Glans, Y. Chen, S. Yan, F. Pan, L. F. Piper, J. Denlinger, J. Guo, Z. Hussain, Y. D. Chuang, W. Yang, *Rev. Sci. Instrum.* **2017**, *88*, 033106.

[37] A. K. Frank de Groot, in *Core Level Spectroscopy of Solids*, CRC Press, **2008**, pp. 11–37.

[38] E. J. McDermott, E. Z. Kurmaev, T. D. Boyko, L. D. Finkelstein, R. J. Green, K. Maeda, K. Domen, A. Moewes, *J. Phys. Chem. C* **2012**, *116*, 7694–7700.

[39] G. Ghiringhelli, N. B. Brookes, E. Annese, H. Berger, C. Dallera, M. Grioni, L. Perfetti, A. Tagliaferri, L. Braicovich, *Phys. Rev. Lett.* **2004**, *92*, 117406.

[40] S. Moser, S. Fatale, P. Krüger, H. Berger, P. Bugnon, A. Magrez, H. Niwa, J. Miyawaki, Y. Harada, M. Grioni, *Phys. Rev. Lett.* **2015**, *115*, 096404.

[41] Y. D. Chuang, Y. C. Shao, A. Cruz, K. Hanzel, A. Brown, A. Frano, R. Qiao, B. Smith, E. Domning, S. W. Huang, L. A. Wray, W. S. Lee, Z. X. Shen, T. P. Devereaux, J. W. Chiou, W. F. Pong, V. V. Yashchuk, E. Gullikson, R. Reininger, W. Yang, J. Guo, R. Duarte, Z. Hussain, *Rev. Sci. Instrum.* **2017**, *88*, 013110.

[42] a) M. Freiwald, S. Cramm, W. Eberhardt, S. Eisebitt, *J. Electron Spectrosc. Relat. Phenom.* **2004**, *137–140*, 413–416; b) M. Nagasaka, H. Yuzawa, T. Horigome, N. Kosugi, *Rev. Sci. Instrum.* **2014**, *85*, 104105; cK. M. Lange, E. F. Aziz, *Chem. Soc. Rev.* **2013**, *42*, 6840–6859.

[43] R. Qiao, Y. Xia, X. Feng, J. Macdougall, J. Pepper, K. Armitage, J. Borsos, K. G. Knauss, N. Lee, A. Allezy, B. Gilbert, A. A. MacDowell, Y. S. Liu, P. A. Glans, X. Sun, W. Chao, J. Guo, *Rev. Sci. Instrum.* **2018**, *89*, 013114.

[44] B. L. Henke, E. M. Gullikson, J. C. Davis, *At. Data Nucl. Data Tables* **1993**, *54*, 181–342.

[45] a) S. Axnanda, E. J. Crumlin, B. Mao, S. Rani, R. Chang, P. G. Karlsson, M. O. M. Edwards, M. Lundqvist, R. Moberg, P. Ross, Z. Hussain, Z. Liu, *Sci. Rep.* **2015**, *5*, 9788; b) W. C. Chueh, A. H. McDaniel, M. E. Grass, Y. Hao, N. Jabeen, Z. Liu, S. M. Haile, K. F. McCarty, H. Bluhm, F. El Gabaly, *Chem. Mater.* **2012**, *24*, 1876–1882.

[46] R. Delmelle, B. Probst, R. Alberto, A. Züttel, D. Bleiner, A. Borgschulte, *Rev. Sci. Instrum.* **2015**, *86*, 053104.

[47] C.-S. Li, G. Melaet, W. T. Ralston, K. An, C. Brooks, Y. Ye, Y.-S. Liu, J. Zhu, J. Guo, S. Alayoglu, G. A. Somorjai, *Nat. Commun.* **2015**, *6*, 6538.

[48] T. V. W. Janssens, H. Falsig, L. F. Lundegaard, P. N. R. Vennestrøm, S. B. Rasmussen, P. G. Moses, F. Giordanino, E. Borfecchia, K. A. Lomachenko, C. Lamberti, S. Bordiga, A. Godiksen, S. Mossin, P. Beato, *ACS Catal.* **2015**, *5*, 2832–2845.

[49] a) A. Tuxen, S. Carenco, M. Chintapalli, C.-H. Chuang, C. Escudero, E. Pach, P. Jiang, F. Borondics, B. Beberwyck, A. P. Alivisatos, G. Thornton, W.-F. Pong, J. Guo, R. Perez, F. Besenbacher, M. Salmeron, *Journal of the American Chemical Society* **2013**, *135*, 2273–2278; b) M. S. Kamal, S. A. Razzak, M. M. Hossain, *Atmos. Environ.* **2016**, *140*, 117–134.

[50] E. de Smit, I. Swart, J. F. Creemer, G. H. Hoveling, M. K. Gilles, T. Tyliszczak, P. J. Kooyman, H. W. Zandbergen, C. Morin, B. M. Weckhuysen, F. M. F. de Groot, *Nature* **2008**, *456*, 222.

[51] a) T. Nakamura, R. Oike, Y. Kimura, Y. Tamenori, T. Kawada, K. Amezawa, *ChemSusChem* **2017**, *10*, 2008–2014; b) Y.-R. Lu, T.-Z. Wu, H.-W. Chang, J.-L. Chen, C.-L. Chen, D.-H. Wei, J.-M. Chen, W.-C. Chou, C.-L. Dong, *Phys. Chem. Chem. Phys.* **2017**, *19*, 14224–14229; c) C. Zhang, J. Gustafson, L. R. Merte, J. Evertsson, K. Norén, S. Carlson, H. Svensson, P.-A. Carlsson, *Rev. Sci. Instrum.* **2015**, *86*, 033112.

[52] L. Zaluski, A. Zaluska, J. O. Ström-Olsen, *J. Alloys Compd.* **1997**, *253–254*, 70–79.

[53] B. Bogdanović, M. Schwickardi, *J. Alloys Compd.* **1997**, *253–254*, 1–9.

[54] K.-F. Aguey-Zinsou, J.-R. Ares-Fernández, *Energy Environ. Sci.* **2010**, *3*, 526–543.

[55] J. Urban, *Fuel Cells Bulletin* **2016**, *2016*, 14.

[56] K. G. Ray, L. E. Klebanoff, J. R. I. Lee, V. Stavila, T. W. Heo, P. Shea, A. A. Baker, S. Kang, M. Bagge-Hansen, Y.-S. Liu, J. L. White, B. C. Wood, *Phys. Chem. Chem. Phys.* **2017**, *19*, 22646–22658.

[57] L. F. Wan, Y.-S. Liu, E. S. Cho, J. D. Forster, S. Jeong, H.-T. Wang, J. J. Urban, J. Guo, D. Prendergast, *Nano Lett.* **2017**, *17*, 5540–5545.